

# Experimental Study on Flexural Behavior of Box Floors with Orthogonal Rib Beams Made of Poplar Laminated Veneer Lumber

Xiangyu Su,<sup>a,b</sup> Jing Chen,<sup>b</sup> Yan Liu,<sup>b,\*</sup> Xufeng Sun,<sup>b</sup> Gong Meng,<sup>c</sup> and Haida Wang<sup>b</sup>

This study examined the flexural behavior of the poplar laminated veneer lumber (LVL) box floor with orthogonal rib beams. Four 3.6 m × 4.8 m box floor samples made of poplar LVL orthogonal rib beams and oriented strand board (OSB) plates were tested under vertical uniform loading, from which the bearing capacity, stiffness, and failure characteristics were analyzed. There was no damage in all box floor samples at the normal service load of 2.5 kN/m<sup>2</sup>, and the maximum deflection was far less than the allowable value. When the maximum load was applied, the load-displacement curve of each floor sample exhibited a linear relationship without obvious failure. However, localized failure was manifested as the dislocation slip of the rib beams relative to the upper and lower floor slabs at the corner nodes and the joint expansion and staggered floors at the bottom plate, with obvious failure signs. The rib beam height had the most significant impact on the floor stiffness, followed by the spacing of short-side rib beams, whereas the OSB plate thickness had least impact. The mid-span deflections of poplar LVL orthogonal ribbed box floor samples, which were calculated using the analog slab method, were in good agreement with the experimental results with an error being less than 10%.

DOI: 10.15376/biores.17.4.6019-6035

*Keywords:* Poplar laminated veneer lumber (LVL); Box floor; Orthogonal rib beam; Static test; Flexural behavior

*Contact information:* a: Management Committee of Hai'an Shanghu Innovation Zone (Sino-Italian Hai'an Ecological Park), Nantong, Jiangsu 226600, China; b: College of Architectural Science and Engineering, Yangzhou University, Yangzhou, Jiangsu 225127, China; c: Wood Science and Technology Center, University of New Brunswick, Fredericton, New Brunswick, E3C 2G6, Canada;

\* Corresponding Author: liuyan@yzu.edu.cn

## INTRODUCTION

In the 1960s and 1970s, China successfully introduced poplar (*Populus euramevicana* cv. I-214) from Italy, and it has become popular in China. After decades of development, the domestic poplar resources are quite rich, and a modern industrial development pattern has been formed, from seed selection and cultivation to expanded reproduction. Poplar laminated veneer lumber (LVL) is widely used in packing materials and furniture components in China. However, it is seldom used in building construction. Therefore, research on the application of poplar LVL in construction will promote the sustainable development of modern timber structures in China. Therefore, the research team has completed a series of studies on the mechanical performance of poplar LVL members, frames, and trusses. This paper mainly introduces the study on the mechanical performance of poplar LVL box floor.

Floor panels are an important component of prefabricated wooden buildings. However, traditional wooden floors composed of girders, grids, cross braces, and floor

slabs have many disadvantages, such as low stiffness, large vibration response, and low comfort. As early as the 1950s, Countryman (1952) studied the effects of floor slab layout, floor slab thickness, and grid connection on the stiffness of wooden floor slabs through the static test. The results showed that the strength of the nail connection between the grid and the floor slab exhibited the most significant effect on the stiffness of wooden floors. Countryman and Colbenson (1954) investigated the effects of floor slab-grid top spacing and depth-span ratio on the lateral stiffness of wooden floors, discovering that nail spacing, nail size, and floor slab thickness were the most influential factors. Zagajeski *et al.* (1984) conducted an experimental study on the in-plane shear response of plywood floors under monotonic and cyclic loads. They analyzed the effects of cross brace, opening, plywood thickness, and nail size on the in-plane shear deformation, noting that repeated loading could reduce the floor stiffness. Johnson (1994) tested the field vibration characteristics of 86 wooden floor samples, analyzed the data, and proposed the comfort standard that the basic frequency should be greater than 15 Hz. Dolan *et al.* (1999) further clarified this standard by tracking the performance of these floor samples and proposed a standard of greater than 14 Hz for occupied wooden floors. Suzuki *et al.* (1995) conducted an excitation test with the vibration exciter and shaking table for an 11.18 by 6.38 m full-scale wooden floor, showing that the shear vibration theory could more accurately calculate the in-plane natural frequency and mode of the wooden floor. Filiatrault *et al.* (2002) also conducted a low-cycle test on the wooden floor of a full-scale two-story wooden frame house to study the influence of floor parameters on in-plane internal stiffness. The results showed that the edge cross brace of the floor slab and the upper and lower walls played the most significant role in improving the in-plane stiffness.

As for the research on structural types of wooden floors, Xiong *et al.* (2012) studied the flexural behavior of composite beams of wood-based structural plates and rectangular-section wood joists through the two-point loading tests of 42 wooden beam samples. They found that the stiffness and flexural capacity were significantly improved when the structure was changed from a rectangular-section beam to a T-shaped composite beam and then to an I-shaped composite beam. Awaludin *et al.* (2017) also conducted full-scale sample bending experiments on LVL wooden floors with various rib beam forms to find the optimum structure. The results showed that the box rib beam floor exhibited better bending stiffness and bearing capacity compared with the I-shaped rib beam floor. Wang (2012) designed a two-way wood truss floor system by substituting the truss for the grid and cross brace and provided improvement measures based on the test analysis. The results revealed that the main factor affecting the floor stiffness and bearing capacity was the cooperation of the trusses in two directions. Xue *et al.* (2019) used herringbone and monoclinic parallel chord trusses as the grid of light wood floors and applied uniform loads to test the bearing performance and deflection. The results showed that the deformations of the two parallel chord trusses were similar at midspan and the ends, which were far lower than the specified deflection limit. Li *et al.* (2016) used C-shaped thin-walled steel members to form a joist and connected the wood plate to the steel joist with screws to form a new steel wood hybrid floor. The in-plane cyclic loading test suggested that the shear deformation of this floor type accounted for 90% of the in-plane deformation. The bearing performance exhibited obvious nonlinear characteristics, and the ductility of the floor was closely related to the failure mode of the threaded connection between the steel joist and wood plate. Loss and Frangi (2017) designed a prefabricated modular steel wood composite floor unit, in which cross-laminated timber (CLT) was used for the wooden floor. Through the in-plane monotonic and cyclic loading tests of the full-scale sample, it was revealed that the deformation of this floor type mainly originated from the connecting

steel joints between beams, which avoided the degradation of material properties in the CLT floor under reciprocating loads.

This study proposed a new type of wooden floor structure with an aim at enhancing the floor stiffness based on the previous studies (Loss and Frangi 2017; Xing 2020). The floor structure proposed adopted two-way orthogonal Poplar LVL rib beams connected by metal components, and the oriented strand board (OSB) as the top and bottom plates to form the box floor. The hollow box structure facilitated heat and sound insulation by filling it with air and reducing the thickness of the floor structure layer. Through the flexural performance tests under local and overall loading, the effects of rib beam depth-span ratio, rib beam spacing, and OSB plate thickness on the mechanical performance of floor slabs were analyzed, providing support for the engineering applications of orthogonal rib beam box floors made of poplar LVL.

## EXPERIMENTAL

### Test Sample Design

Figure 1 illustrates the floor structure designed in this study. Four types of 3600 mm × 4800 mm planar poplar LVL box floor samples were designed and manufactured by the research group according to the Standard for Design of Timber Structures (GB 50005 2017). Each type had one sample that was built and tested. The distance between the long-side rib beams was 600 mm in all samples. The other structural parameters and component layout are illustrated in Table 1 and Fig. 2.

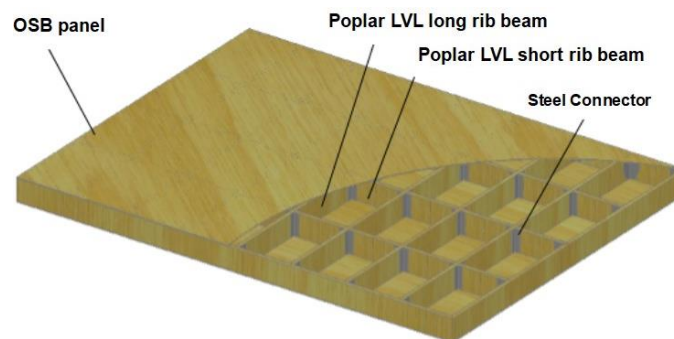
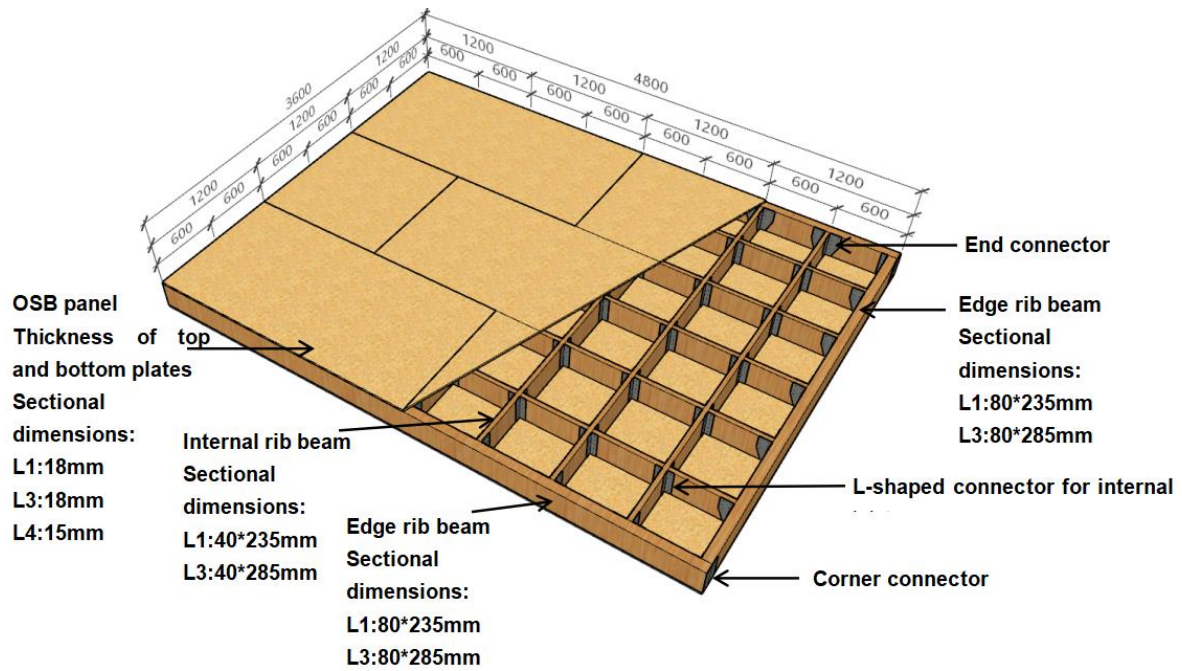


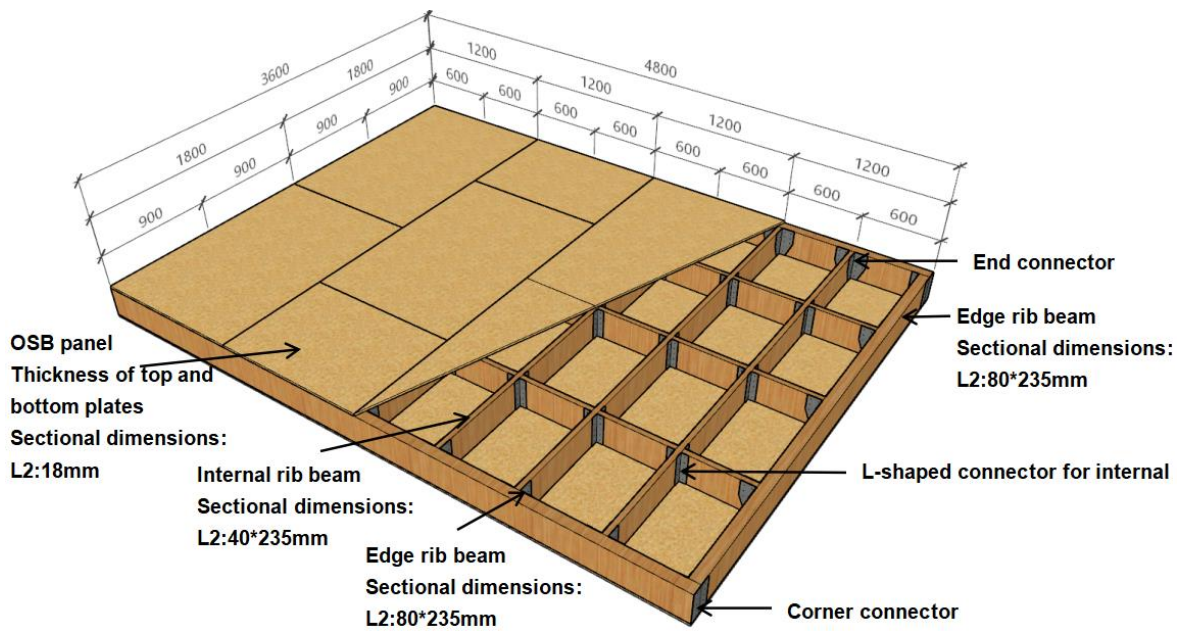
Fig. 1. Orthogonal rib beam box floor made of poplar LVL

Table 1. Parameters of the Floor Sample

No.	Short-side Rib Beam Spacing (mm)	Rib Beam Cross-section Size (mm)	OSB Plate Thickness (mm)
L1	600	40 × 235	18.3
L2	900	40 × 235	18.3
L3	600	40 × 285	18.3
L4	600	40 × 235	15.1



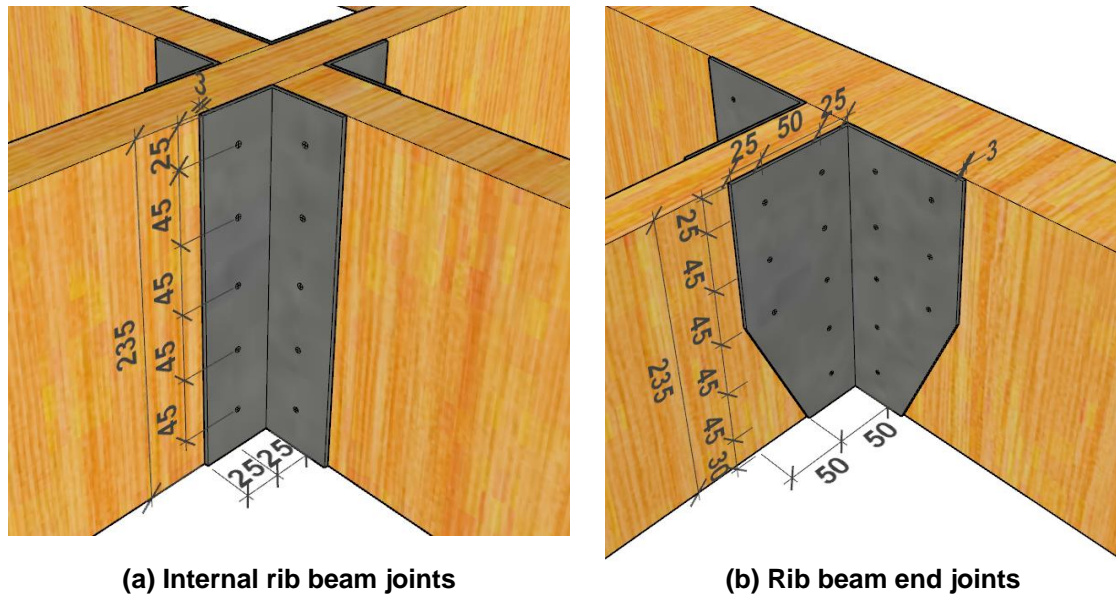
(a) Samples L1, L3, L4



(b) Sample L2

**Fig. 2.** Layout details of the floor components

The internal rib beam joints of each sample adopted the 3 mm thick Q235 steel L-shaped connector, which was connected by  $M4 \times 20$  mm cross-countersunk self-tapping screws. The size of connectors and the number of screws were increased at the end nodes of the rib beam, which were connected to the edge-sealing rib beam by  $M4 \times 40$  mm cross-countersunk self-tapping screws (Liu *et al.* 2022). The node structure is detailed in Fig. 3.



(a) Internal rib beam joints

(b) Rib beam end joints

**Fig. 3.** Structural details of the node connector

OSB plates were used as the upper and lower floor slabs of the box floor, which were connected to the rib beam by  $2.8 \times 50$  mm round nails. The spacing between the round nails was 150 mm and 300 mm at the edge-sealing rib beam and the internal rib beam, respectively. The installed floor sample is displayed in Fig. 4.



(a) Sample rib beam



(b) Sample after installation of top and bottom plates

**Fig. 4.** Floor sample after installation

The poplar LVL used in this study was purchased from Jiangsu Jiuhe Timber Company (Jiangsu, China), and the OSB, nails, and cross countersunk head tapping screws were all purchased from a local market. The 3 mm thick Q235 steel L-joint was processed with the help of Yangzhou Huayun Electric Co., Ltd. (Jiangsu, China).

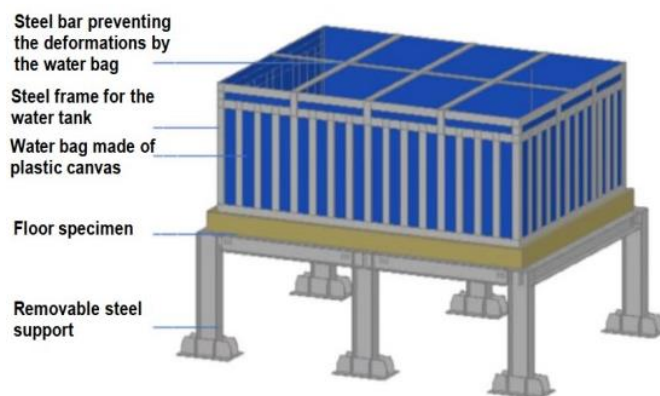
The physical and mechanical properties of poplar LVL based on the experimental results (Liu *et al.* 2017) were used for the rib beam (Table 2).

**Table 2.** Physical and Mechanical Parameters of Poplar LVL

Water content (%)		12.8
Density (g/cm <sup>3</sup> )		0.576
Tensile strength parallel to grain (MPa)		39.4
Compressive strength parallel to grain (MPa)		37.03
Compressive strength perpendicular to grain (MPa)		6.3
Flexural strength (MPa)	Horizontal	61.56
	Vertical	64.8
Flexural modulus of elasticity (MPa)	Horizontal	9877
	Vertical	10135

### Loading Scheme

A self-designed water tank was used for the loading test, which was composed of a steel frame and a thickened flexible plastic canvas water bag, as displayed in Fig. 5. The clear height of the steel frame was 1500 mm, and the clear height of the canvas water bag was 1600 mm. The reserved 100 mm height difference could allow fitting of the water bag and roof during the loading process so that the load could act evenly on the floor sample and roof during the loading process so that the load could act evenly on the floor sample and allow the bag to deform with the floor (Xing 2012).



(a) Schematic of the loading device



(b) Installed loading device



(c) Interior of the water tank when loading

**Fig. 5.** Loading device

A multi-stage loading process was adopted according to GB/T 50329 (2012) and ASTM E2322-03 (2015). First, 5% of the ultimate load (the ultimate load here was estimated by finite element analysis) was preloaded and held for 15 min. During this time, check to see if the instruments are working properly, and then empty the water tank for unloading. During formal loading, the load was set at 10% of the ultimate load for the first level and increased by 5% of the ultimate load for each new level. The holding time was fixed at 15 min, and the data were recorded when the reading of the measuring instrument was stable.

**Layout of Measuring Points**

The symmetry in load and structure of the box floor was considered in the test. All the displacement gauges were arranged below the rib beam node, and the layouts of displacement gauges for samples L1 through L4 are illustrated in Fig. 6.

Strain gauges were installed on the bottom plate, which were arranged at the central axis considering the sample symmetry, as displayed in Fig. 7.

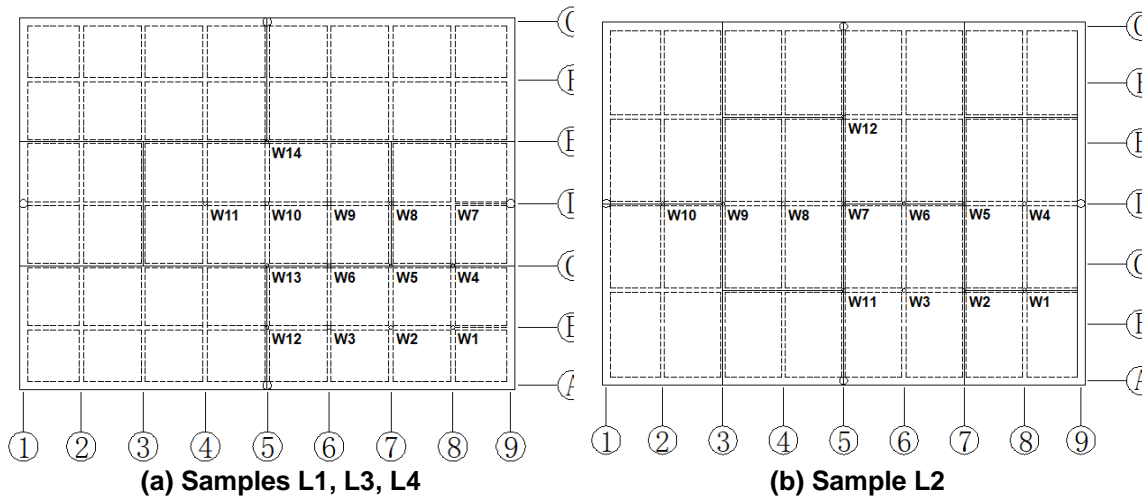


Fig. 6. Layout of displacement measuring points

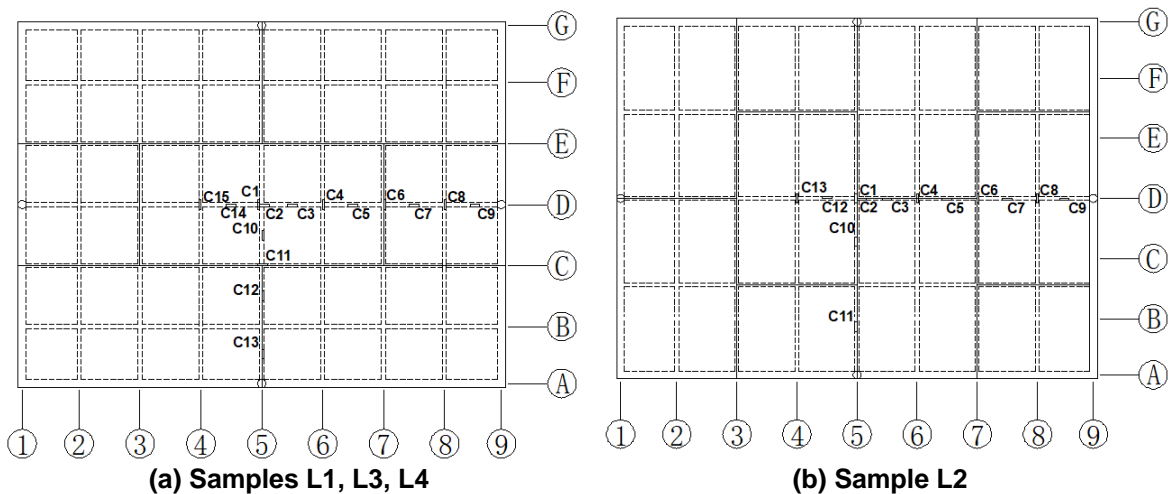


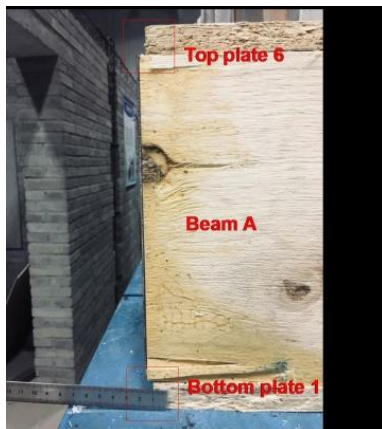
Fig. 7. Layout of strain measuring points

## RESULTS AND DISCUSSION

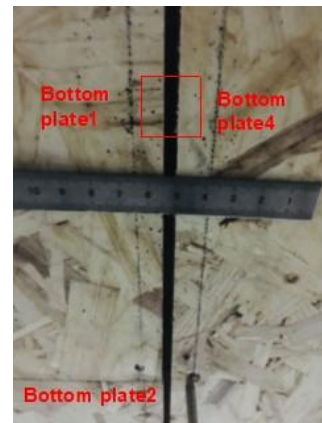
### Failure Morphology

No damage was present when the load was set to the standard GB 50009-2012 (2012) normal floor service load of  $2.5 \text{ kN/m}^2$ . Considering the reliability and safety of the test device, the test was terminated when the load was  $15 \text{ kN/m}^2$  for samples L1, L3, and L4 and  $13 \text{ kN/m}^2$  for sample L2. The following paper only discussed the test phenomena when the samples were loaded to the levels mentioned above.

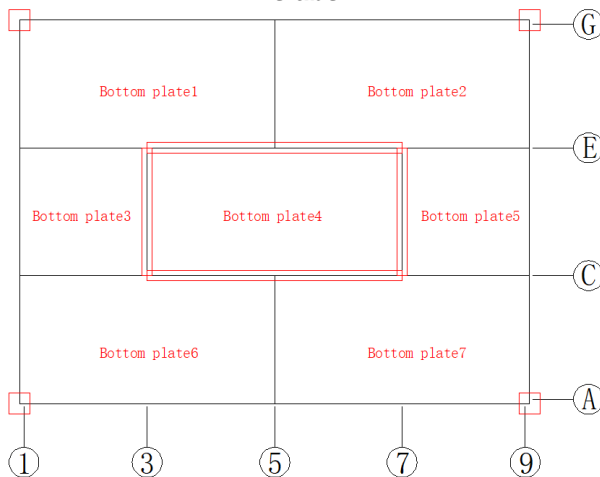
1) Sample L1: When the load reached  $12 \text{ kN/m}^2$ , a few nail joints at the bottom of the midspan of the specimen began to fail, and a continuous sound came from the floor slab. With the increase of flexural deformation as the load was increased to  $15 \text{ kN/m}^2$ , dislocation slip appeared between the beam ends at the four corner nodes and the upper and lower floor slabs, as illustrated in the red square boxes in Fig. 8a. All local damage parts are also labelled using the red boxes in the following figures. In the meantime, expansions with a width of 5 to 7 mm appeared at the joints of multiple bottom plates (Fig. 8b), and their positions are displayed in Fig. 8c. Many connectors were separated from the rib beam, and the screws at A-5 were pulled out (Fig. 8d) after unloading and removing the upper and lower floor slabs. The specific locations are displayed in Fig. 8e.



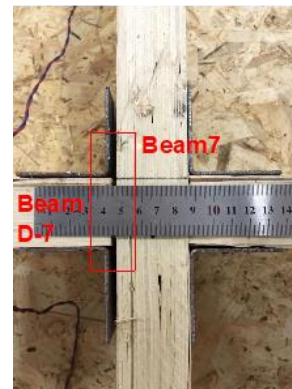
(a) Dislocation slip of upper and lower floor slabs



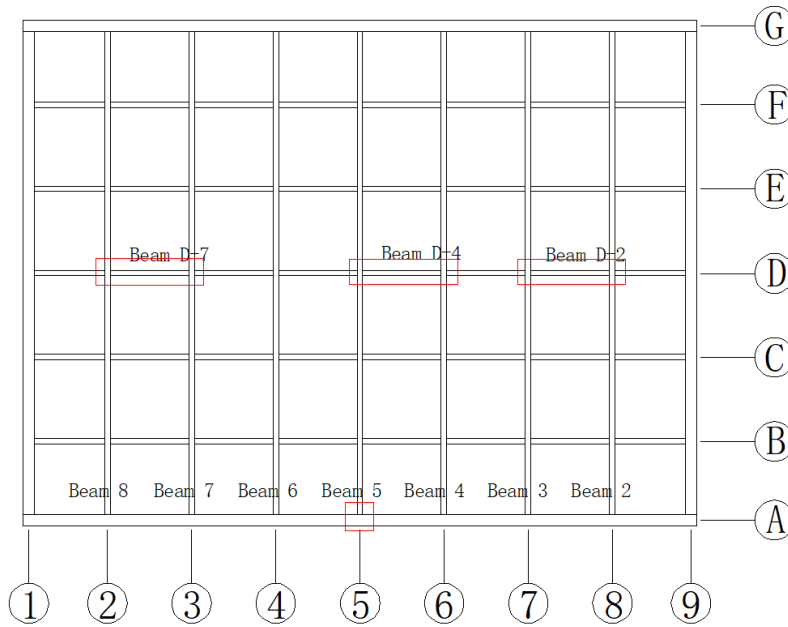
(b) Floor joint expansion



(c) Locations of floor joint expansion



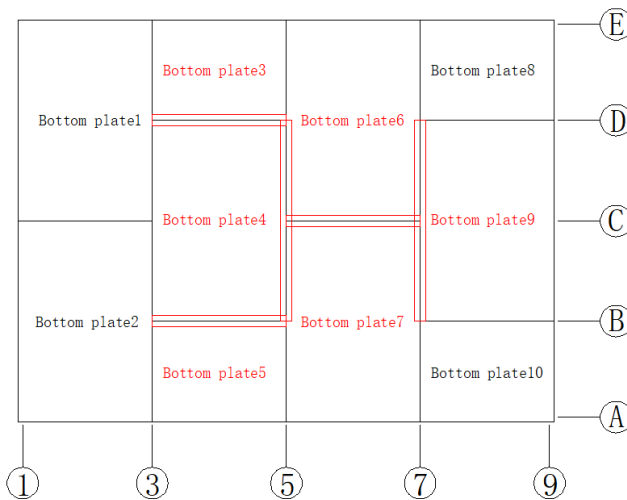
(d) The connector was separated from the rib beam and the screws were pulled out



(e) The position where the connector was separated from the rib beam

Fig. 8. Locations and failure in Sample L1

2) Sample L2: When the load was 13 kN/m<sup>2</sup>, expansions with a width of 4 to 7 mm occurred at several bottom plate joints, as displayed in Fig. 9a. The camera placed inside the floor observed that the bottom plate was separated from the rib beam, resulting in staggered layers of about 3 mm at multiple joints (Fig. 9b). After removing the upper and lower floor slabs, many connectors were separated from the rib beam. Some gaps appeared at the rib beam joints, and the screws at A-5 were pulled out. The specific locations are displayed in Fig. 9c.



(a) Locations of floor joint expansion



(b) Staggered layers at the bottom plate joints

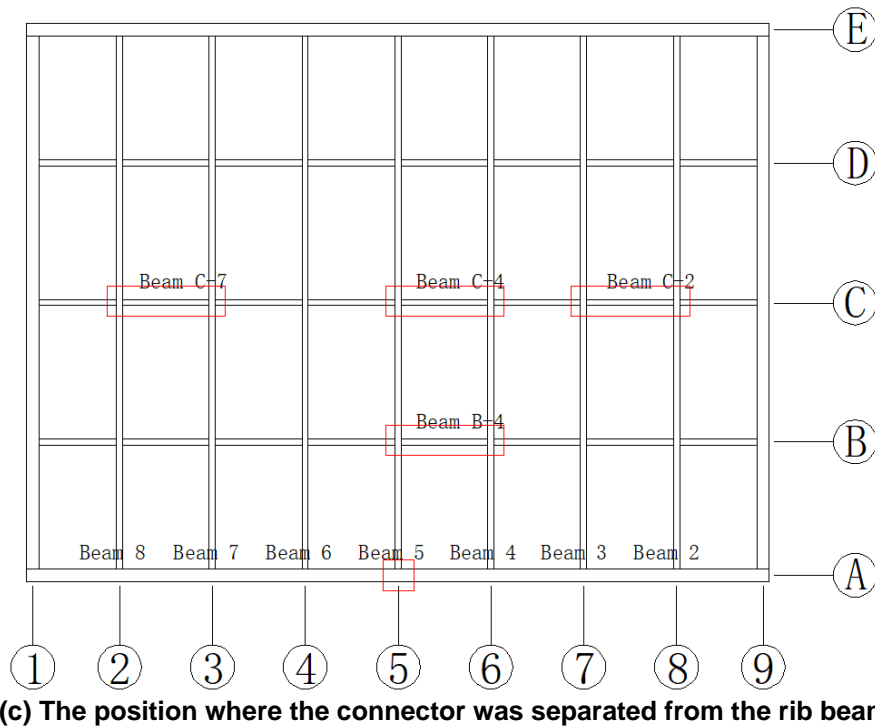


**Fig. 9.** Location and failure in Sample L2

3) Sample L3: The overall stiffness increased as the height of the rib beam increased in this sample. Therefore, when the load was  $15 \text{ kN/m}^2$ , no obvious damage appeared except for the dislocation slip of about 4 mm between the beam ends and the upper and lower floor slabs at the four corner nodes, as shown in Fig. 10. After removing the upper and lower floor slabs that the beam end gap, the connector separated from the wood beam D-7 and beam D-2, and partially pulled screws at A-5 were present close to the edge-sealing rib beam rather than the middle rib beam node.

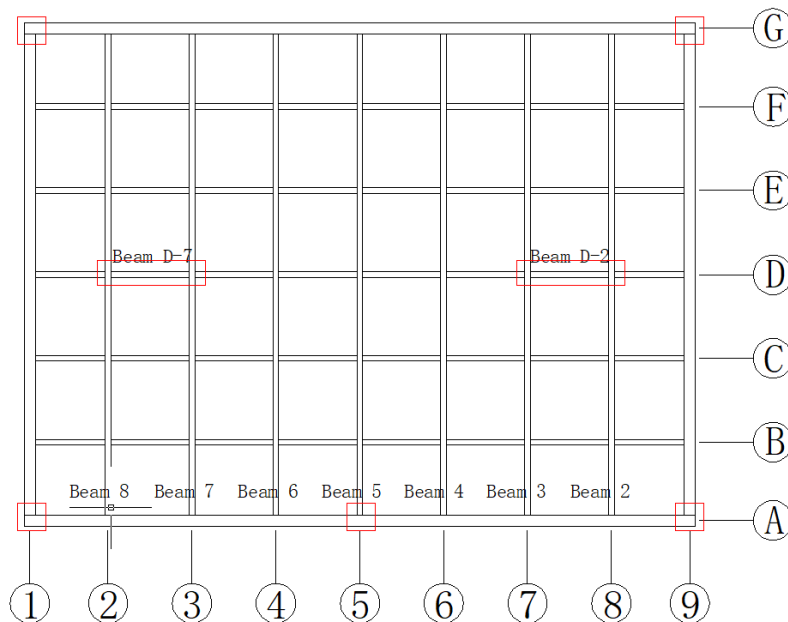


**Fig. 10.** Location of failure in Sample L3

4) Sample L4: The failures of sample L4 were similar to those of sample L1. When loaded to  $15 \text{ kN/m}^2$ , dislocation slip occurred between the beam ends and the upper and lower floor slabs at the four corners, as illustrated in Fig. 11a, and expansions in the range of 5 to 7 mm appeared at the joints of multiple floor slabs. However, the OSB plate in this sample was thinner than that of sample L1. After removing the upper and lower floor slabs, in addition to the beam end gap, the separation of the connector from the wood beam and partially pulled screws at the positions displayed were observed. Sunken rib beams were also observed at the joints between beam D-5 and beam 6, beam D-4 and beam 4, with a sunken distance of 2 and 3 mm, respectively (Fig. 11b).

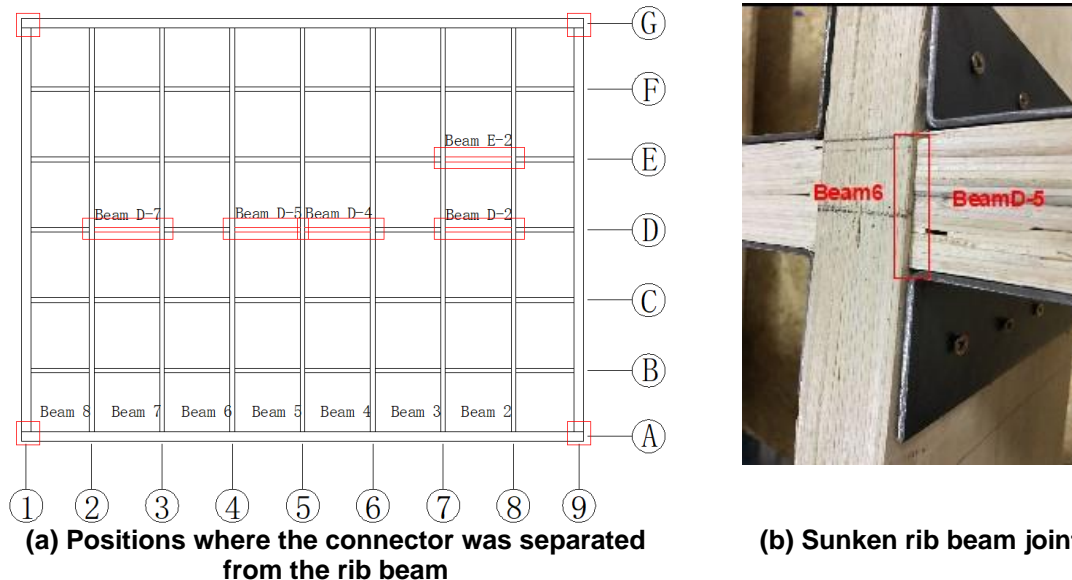


Fig. 11. Location and failure in Sample L4

No overall failure was present at the maximum load. Except for sample L3, the other samples exhibited different degrees of joint expansion, partial pulling out of nails, and staggered layers between the bottom plates. These results revealed that when metal connectors and self-tapping screws with good ductility and easy deformation were used at the joints, the failure of the box floor sample was manifested as the joint expansion and staggered layers in the middle of the bottom plate. Thus, it showed obvious signs of failure.

### Load-displacement Relationship

Figure 12 presents the load displacement curves of samples L1 and L4 and the deflection distributions after symmetrical expansion when loaded to  $15 \text{ kN/m}^2$ . The deflection of symmetrical measuring points were basically the same for each floor sample, reaching the maximum deflection in both directions at the midpoint and gradually decreasing from the midpoint to the four sides. This bowl-shaped change indicated that the two-way slab effect was relatively significant. Furthermore, the load displacement curve was basically linear when loaded to the maximum value, indicating that the poplar LVL box floor sample exhibited high stiffness and good integrity.

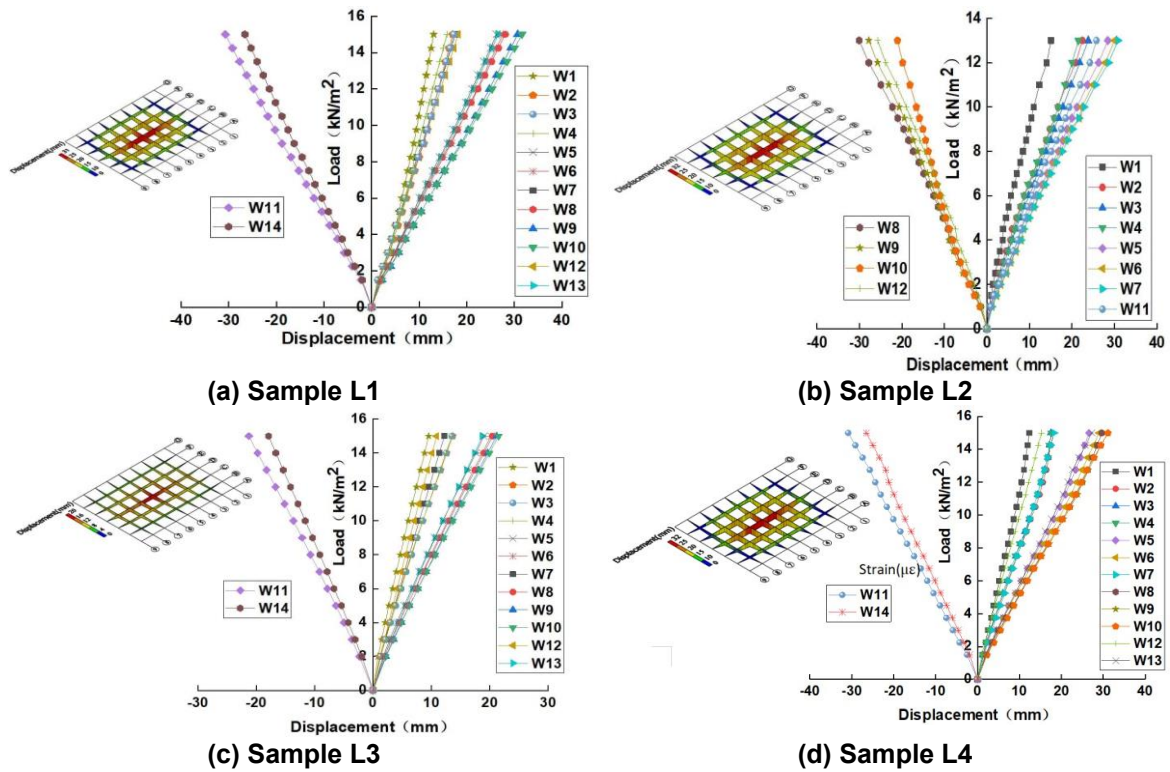


Fig. 12. Load–displacement curves and deflection distributions of the floor samples

Figure 13 compares the load displacement curves at the midpoint of the samples, displaying the following characteristics: 1. When the load was 2.5 kN/m<sup>2</sup>, the standard value of normal floor service load, the maximum deflections of samples L1 and L4 were 4.57, 5.79, 3.00, and 4.80 mm, respectively, which were far less than the allowable value of  $1/250 = 14.40$  mm by GB 50005-2017 (2017) Standard for Design of Timber Structures; 2.

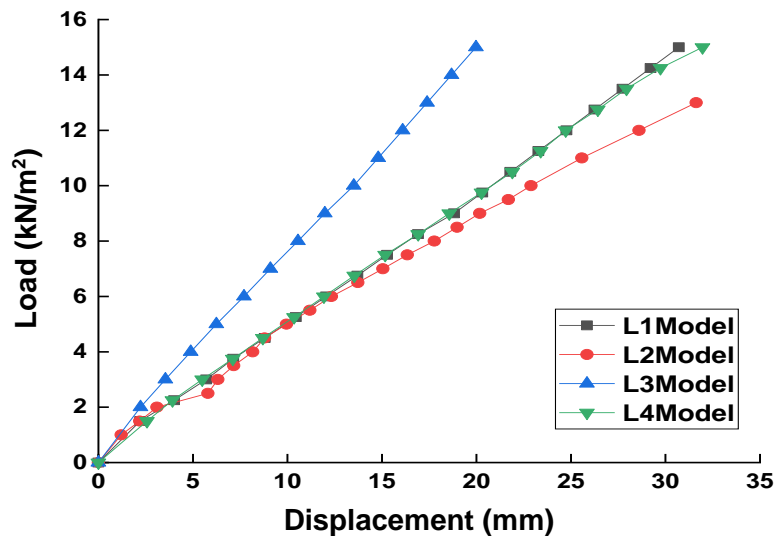


Fig. 13. Comparison of load–displacement curves of the samples

Compared with sample L1, under a load level of  $2.5 \text{ kN/m}^2$ , the deflection changes of samples L2–L4 were +26.7%, –34.4%, and +5.0%, respectively, indicating that the change in rib beam height had the greatest impact on floor stiffness, followed by the spacing between short-side rib beams, and the OSB floor slab thickness had little impact. Since the flexural deformation under uniform load was close to the first-order vibration mode of the floor, the first-order natural frequencies of samples L1 and L4 could be calculated as about 21.64, 20.33, 25.70, and 22.10 Hz, respectively, according to the measured deflections. These values met the requirement that the natural frequency for floor comfort should not be less than 3 Hz specified in Reference JGJT 441-2019 (2019).

Figure 14 shows the load-strain curve of the measuring points at the base plate of each sample. The comparison led to the following conclusions: 1. The stiffness of each sample's base plate material decreased after loading to  $3.0 \text{ kN/m}^2$ . For samples L1, L2, and L3, when the load level reached 9.5, 10.0, and  $6.0 \text{ kN/m}^2$ , respectively, the rise in strain began to slow down with the increasing load. Combined with the test phenomena of joint expansion and staggered layers between the bottom plates, it meant that some nails in the bottom plate began to be pulled out, resulting in the relative slip between the bottom plate and rib beam and their weak collaborative deformation ability. As for sample L4, when the load reached  $10.0 \text{ kN/m}^2$ , the increase in strain started to accelerate with the increase in load. This was because the decrease in OSB plate thickness increased the embedded depth of nails, strengthening the nail joints and making the bottom plate enter the yield phase.

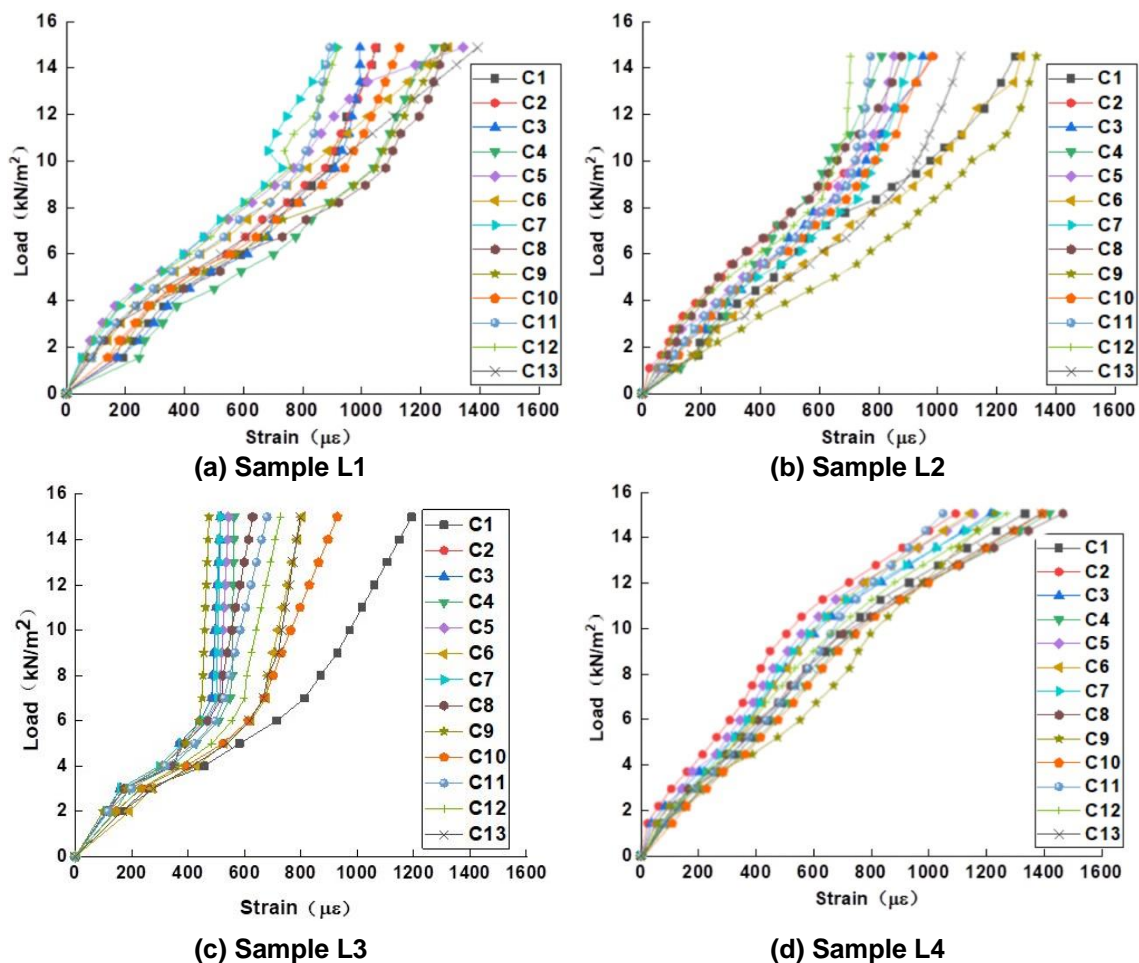


Fig. 14. Load–strain curves of measuring points at the bottom plates for the floor samples

Previously, poplar LVL orthogonal rib beam floor was tested without the floor panel (Xing 2020; Yang 2020). Under the same parameters, the deflection of the floor without floor slabs was 108.3% higher than that of the box floor under the normal service load when the rib beam height was 235 mm. This increase in deflection was 86.3% when the height of the rib beam was 285 mm. This showed that the upper and lower OSB floor slabs played a critical role in improving the floor stiffness.

### Mid-point Deflection Estimation

The deflection of poplar LVL orthogonal ribbed box floor can be theoretically calculated and analyzed by using three different theoretical calculation methods: cross beam system, two-way slab, and pseudo-plate method. The results show that the pseudo-plate method has the maximum integrity and can be applied to the theoretical analysis of sandwich structures (Hong *et al.* 2018; Wang 2021). This study used the pseudo plate method (Hong *et al.* 2018) to calculate the deflections of orthogonal rib beam box floors and analyze its applicability. If the poplar LVL box floor is equated with an orthotropic plate, its bending and torsional stiffness can be calculated using Eq. 1,

$$\begin{cases} D_1 = \frac{EI_x}{c_1} \\ D_2 = \frac{EI_y}{c_2} \\ D_3 = \frac{2Eh_b^3}{12(1-\nu^2)} + 0.5G\left(\frac{J_{tx}}{c_1} + \frac{J_{ty}}{c_2}\right) \end{cases} \quad (1)$$

where  $D_1$  and  $D_2$  are the bending stiffnesses in  $x$  and  $y$  directions, respectively;  $E$  is the elastic modulus;  $I_x$  and  $I_y$  are the moments of inertia for the floor section in the two directions relative to the neutral axis;  $c_1$  and  $c_2$  are the rib beam spacings in the two directions;  $D_3$  is the torsional stiffness, calculated separately and then added for the plate and the beam;  $h_b$  is the OSB plate thickness;  $\nu$  is Poisson's ratio;  $G$  is the shear modulus;  $J_{tx}$  and  $J_{ty}$  are the torsional stiffnesses of the rib beam in  $x$  and  $y$  directions, respectively, which are calculated according to Eq. 2,

$$\begin{cases} J_{tx} = \frac{b_1h_1^3 + b_1^3h_1}{12} \\ J_{ty} = \frac{b_2h_2^3 + b_2^3h_2}{12} \end{cases} \quad (2)$$

where  $b_1$  and  $b_2$  are the rib beam widths in the two directions and  $h_1$  and  $h_2$  are the rib beam heights in the two directions.

According to the elastic plate theory, the differential equation of the orthotropic plate under transverse load is shown in Eq. 3.

$$D_1 \frac{\partial^4 f}{\partial x^4} + D_2 \frac{\partial^4 f}{\partial y^4} + 2D_3 \frac{\partial^4 f}{\partial x^2 \partial y^2} = q \quad (3)$$

If a plate simply supported on four sides is considered, the series solution of Eq. 3 can be expressed as follows.

$$f = \frac{16q_0}{\pi^6} \sum_m^{\infty} \sum_n^{\infty} \frac{\sin\left(\frac{m\pi x}{a}\right) \sin\left(\frac{n\pi y}{b}\right)}{mn \left( \frac{D_1 m^4}{a^4} + \frac{2D_3 m^2 n^2}{a^2 b^2} + \frac{D_2 n^4}{b^4} \right)} \quad (4)$$

( $m, n = 1, 3, 5, \dots$ )

Table 3 lists the solutions from the pseudo slab method of the midpoint deflection ( $m, n = 1$ ) and its errors relative to the test values when the standard value of normal service load of 2.5 kN/m<sup>2</sup> was set for the floor. The deflection errors estimated using the pseudo slab method under normal service load were less than 10%, which indicated that the pseudo slab method was applicable to the calculation of deflections of a poplar LVL orthogonal rib beam box floor. Such a small error also meant that this type of floor had strong integrity.

**Table 3.** Mid-point Deflection Calculated by the Three Analogue Slab Methods

No.	Calculated value (mm)	Test value (mm)	Error (%)
L1	4.55	4.57	-0.4
L2	6.13	5.79	+5.9
L3	2.75	3.00	-8.3
L4	4.89	4.80	+1.9

## CONCLUSIONS

1. Under the normal floor service load of 2.5 kN/m<sup>2</sup>, the box floor showed no damage. When the load reached the maximum load level in the test, the load–displacement curve still exhibited a linear relationship without obvious failure in each floor sample. The localized failure was manifested in the dislocation slip between the beam ends and the upper and lower floor slabs at the corner nodes, joint expansion, and staggered floors at the bottom plate, separation between the beam end connector and the wooden beam, and partial pulling out of screws.
2. The maximum deflection of each sample under the normal floor service load was far less than the allowable value. The rib beam height had the greatest impact on floor stiffness, followed by the spacing of short-side rib beams, whereas the OSB floor slab thickness had little impact. In comparison with the floor specimens without OSB plates, the “skin effect” of the upper and lower OSB plates improved the floor stiffness. The first-order longitudinal natural frequency obtained by each sample according to the measured deflection met the requirement of natural frequency for floor comfort.
3. The experimental results demonstrated that the poplar LVL orthogonal rib beam box floor possessed good stiffness and bearing capacity, which could provide a new choice for the construction of light timber floors.

## ACKNOWLEDGMENTS

This research project was funded by the National Natural Science Foundation of China, Grant No. 51878590.

## REFERENCES CITED

- ASTM E2322-03 (2015). “Standard test method for conducting transverse and concentrated load tests on panels used in floor and roof construction,” ASTM International, West Conshohocken, PA, USA.
- Awaludin, A., Firmanti, A., Muslikh, Theodarmo, H., and Astuti, D. (2017). “Wood frame floor model of LVL *Paraserianthes falcataria*,” *Proced. Eng.* 171, 113-120. DOI: 10.1016/j.proeng.2017.01.317
- Countryman, D. (1952). *Lateral Tests on Plywood Sheathed Diaphragms: Laboratory Report No. 55*. Douglas-Fir Plywood Association, Tacoma, WA, USA.
- Countryman, D., and Colbenson, P. (1954). *Horizontal Plywood Diaphragm Tests: Laboratory Report No. 63*, Douglas-Fir Plywood Association, Tacoma, WA, USA.
- Dolan, J. D., Murray, T. M., Johnson, J. R., Runte, and Shue, B. C. (1999). “Preventing annoying wood floor vibrations,” *J. Struct. Eng.* 125, 19-24. DOI: 10.1061/(ASCE)0733-9445(1999)125:1(19)
- Filiatrault, A., Fischer, D., Folz, B., and Uang, C. M. (2002). “Experimental parametric study on the in-plane stiffness of wood diaphragms,” *Canad. J. Civil Eng.* 29, 554-566. DOI: 10.1139/102-036
- GB 50005-2017 (2017). “Standard for design of timber structures,” China Architecture and Building Press, Beijing, China.
- GB 50009-2012 (2012). “Load code for the design of building structures,” China Architecture and Building Press, Beijing, China.
- GB/T 50329-2012 (2012). “Standard for test methods of timber structures,” China Architecture and Architecture Press, Beijing, China.
- Hong, J., Liu, W., Fang, H., and Zhang F. (2018). “Stress analysis of composite sandwich panels under unidirectional bending,” *Eng Mech* 35, 41-51.
- JGJT 441-2019 (2019). “Technical standard for human comfort of the floor vibration,” China Architecture and Architecture Press, Beijing, China.
- Johnson, J. R. (1994). *Vibration Acceptability in wood Floor Systems*, Ph.D. Dissertation, Virginia Polytechnic Institute and State University, Blacksburg, VA, USA.
- Li, Z., He, M., Ma, Z., Wang, K., and Renle (2016). “In-plane behavior of timber-steel hybrid floor diaphragms: Experimental testing and numerical simulation,” *J. Struct. Eng.* 142, 04016119.
- Liu, Y., Wang, H., Ding, P., and Song, Y. (2017). “The physical and mechanical properties of the poplar LVL,” *China Forest Prod. Industr.* 44, 12-16. DOI: 10.19531/j.issn1001-5299201702003
- Liu, Y., Chen, J., Ma, H., Gong, M., and Zhang, L. (2022). “Mechanical performance of three types of connections used in orthogonal ribbed beams made of poplar LVL,” *BioResources* 17(3), 4638-4655. DOI:10.15376/biores.17.3.4638-4655
- Loss, C., and Frangi, A. (2017). “Experimental investigation on in-plane stiffness and strength of innovative steel-timber hybrid floor diaphragms,” *Eng. Struct.* 138, 229-244. DOI: 10.1016/j.engstruct.2017.02.032
- Suzuki, S., Fujino, E., and Noguchi, H. (1995). “In-plane dynamic characteristics of wooden diaphragms,” *Struct. Constr. Eng. Trans. AIJ* 60, 119-126. DOI: 10.3130/aijs.60.119\_1
- Wang, B. (2012). *Research on Bearing Capacity of Bidirectional Wood Truss Floor*, Master’s Thesis, Harbin Institute of Technology. DOI: 10.7666/d.D238763
- Wang, H. (2021). *Experimental Study on Flexural Behavior of Poplar LVL Orthogonal Rib Beam Box Floor*, Master’s Thesis, Yangzhou University, Yangzhou, China. DOI:

10.27441/d.cnki.gyzdu.2021.001772

- Xing, L. (2020). *Experimental Study on Flexural Performance of Orthogonal Ribbed Beams with Different Height-span Ratios in Poplar LVL Box Floor*, Master's Thesis, Yangzhou University, Yangzhou, China. DOI:10.27441/d.cnki.gyzdu.2020.000546
- Xiong, H., Kang, J., and Lu, X. (2012). "Bending tests investigation on composite timber beam," *Tongji Univers. Nat. Sci.* 40, 522-528. DOI: 10.3969/j.issn.0253-374x.2012.04.004
- Xue, S., Zhang, Z., and Zhou, H. (2019). "Load bearing test of parallel chord truss of light wooden covering," *Wood Industr.* 33, 1-5. DOI: 10.19455/j.mcgy.20190601
- Yang, X. (2020). *Research on Flexural Performance of Orthogonal Ribbed Girders with Poplar LVL at Different Spacing in Box Floor*, Master's Thesis, Yangzhou University, Yangzhou, China. DOI:10.27441/d.cnki.gyzdu.2020.000706
- Zagajeski, S. W., Halvorsen, G. T., Gangarao, H., Luttrell, L. D., and Jewell, R. B. (1984). *Theoretical and Experimental Studies on Timber Diaphragms Subject to Earthquake Loads* (NSF/CEE-84081), West Virginia University, Morgantown, WV, USA.

Article submitted: July 17, 2022; Peer review completed: August 28, 2022; Revised version received and accepted: September 3, 2022; Published: September 8, 2022.

DOI: 10.15376/biores.17.4.6019-6035